J Mater Sci (2012) 47:797–803
DOI 10.1007/s10853-011-5857-1

Electronic and magnetic properties of $Fe_{3-x}Cr_xSi$ ordered alloys from first principles

Bothina Hamad · Jamil Khalifeh · Qing-Miao Hu · Claude Demangeat

Received: 21 April 2011 / Accepted: 6 August 2011 / Published online: 23 August 2011

Abstract Density functional theory calculations are performed to investigate the electronic and magnetic properties of $Fe_{3-x}Cr_xSi$ alloys with Cr concentration in the range of $0.25 \leq x \leq 2.75$. The $L2_1$ phase is found to be a more stable one in comparison with the A15 phase for $x \leq 1.50$ beyond which the A15 phase becomes more stable. Alloys with the stable $L2_1$ phase are found to be metallic for $x \leq 0.75$, however, a half metallic behavior is found at $x = 1.00$, 1.25, and 1.50 with band gaps of 0.60, 0.24, and 0.21 eV, respectively. In contrast, all A15 structures are found to be metallic. The total magnetic moments are found to decrease for $L2_1$ phase from 14.4 μ_B/cell at $x = 0.25$ to zero at $x = 2.00$ with non-integer values for the metallic structures and integer values for the half-metallic. However, a monotonic decrease is found for the case of A15 phase with values larger than those of $L2_1$ phase.

Introduction

Transition-metal silicides such as Cr_3Si and Fe_3Si binary alloys have stimulated intensive studies over the last few decades due to their significance in integrated circuits technology. The interest in these alloys is related to their metallic behavior and oxidation resistance. Neutron powder diffraction measurements have shown that Cr_3Si alloy crystallizes in A15 structure of the space group $Pm\bar{3}n$ (223) with a lattice constant 4.60 Å [1]. This alloy structure was confirmed to be stable in a temperature range down to 6 K [2, 3] with a Pauli paramagnetic behavior in the temperature range between 4.2 and 300 K [4]. The cubic unit cell of Cr_3Si alloy contains two Si atoms at (0,0,0) and (1/2, 1/2,1/2), and six Cr atoms at (1/4,0,1/2), (1/2,1/4,0), (0,1/2, 1/4), (0,1/2,3/4), (1/2,3/4,0), and (3/4,0,1/2), see Fig. 1.

In contrast, Fe_3Si binary alloy crystallizes in the DO3 structure of the space group $Fm\bar{3}m$ (225). This structure is a cubic superstructure, which is composed of four interpenetrating FCC sublattices, A, B, C, and D, centered at (0, 0, 0), (1/4, 1/4, 1/4), (1/2 , 1/2 , 1/2), and (3/4 , 3/4 , 3/4), Fig. 1. Each A atom is at the center of a cube of four B and four D atoms. In this alloy, Fe atoms occupy two inequivalent sites [A, C] and [B] sites, and Si atoms occupy [D] sites. It has a lattice constant of 5.65 Å [5] and a ferromagnetic behavior with a total magnetic moment of 4.80 μ_B/f.u. [6], which is well compared to our recent predicted value of 4.96 μ_B/f.u. [7]. The Curie temperature (T_c) of this alloy is about 840 K [8].

As these two alloys exhibit completely different geometrical structures and magnetic states, one may expect different electronic, magnetic and geometrical structures upon alloying a parent binary alloy by the transition metal of the other, i.e., doping Fe_3Si binary alloy with Cr atoms or vice versa. Zaleski et al. [9] have measured the magnetization of doped Cr_3Si by Fe. They found that the $Cr_{3-x}Fe_xSi$ alloys change from the nonmagnetic state for $x \leq 0.2$ to the ferromagnetic state at $x = 0.3$. The observed

B. Hamad (✉) · J. Khalifeh
Department of Physics, University of Jordan,
Amman 11942, Jordan
e-mail: b.hamad@ju.edu.jo

Q.-M. Hu
Shenyang National Laboratory for Materials Science,
Institute of Metal Research, Chinese Academy of Sciences,
72 Wenhua Road, Shenyang 110016, China

C. Demangeat
UFR de Physique et d'Ingéniérie, 3 rue de l'Université,
67000 Strasbourg, France

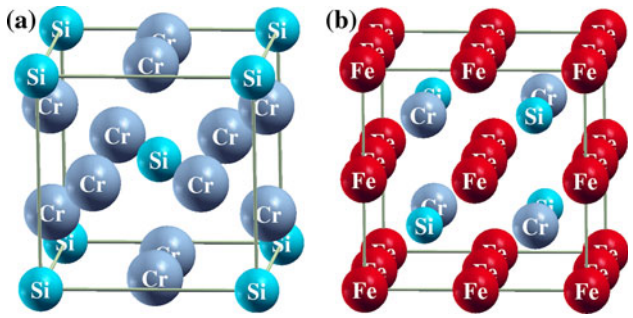

Fig. 1 *Left* The A15 structure of Cr_3Si: Si atoms occupy (0,0,0) and (1/2,1/2,1/2) sites, and Cr atoms occupy (1/4,0,1/2), (1/2,1/4,0), (0,1/2,1/4), (0,1/2,3/4), (1/2,3/4,0), and (3/4,0,1/2) sites. *Right* The DO3 structure of Fe_3Si, where Fe atoms occupy A(0,0,0), B(1/4,1/4,1/4), and C(1/2,1/2,1/2) sites; Si atoms are at D(3/4,3/4,3/4) sites

magnetic moments, however, are weak, while the Curie temperatures are relatively high. The Curie temperature of the sample with $x = 0.2$ was found to be about 320K [9]. A recent experimental study by Goripati et al. [10] has shown an enhancement in the spin polarization of Co_2FeSi by substituting Fe by Cr, which leads to a higher magnetoresistance (MR) value.

As Fe_3Si (DO3 structure) is alloyed with Cr, the B sites are progressively filled until reaching the stoichiometric Fe_2CrSi structure, where all B sites are occupied by Cr atoms. This structure is referred to as a full Heusler alloy ($L2_1$ structure). This alloy has a Curie temperature above room temperature (520 K) [11]. The predicted spin polarization has been found to be very high, 100% [11] (98% [12]) and the total magnetic moment is close to that derived using the Slater-Pauling formula [13] of 2.00 μ_B/f.u. [11] (1.98 μ_B/f.u. [12]) . The saturation magnetic moment at 5 K has been reported as 2.05 μ_B/f.u. [11], which is consistent with the predicted values and those derived from Slater-Pauling formula. In addition, Fe_2CrSi films on MgO substrates have also shown high Curie temperatures, which makes them promising for high-performance magnetic random access memory devices [12]. Recently, Ko et al. [14] have performed a combined theoretical and experimental study to investigate the electronic and magnetic structures of Fe_2CrSi and Cu_2CrSi bulk alloys as well as Fe_2CrSi/Cu_2CrSi interfaces. They found that Fe_2CrSi is ferromagnetic, whereas Cu_2CrSi is nonmagnetic. However, both systems have high density of states at the Fermi level in the majority spin band. Their majority spin bands match very good at the Fermi level leading to a high spin polarization of 80%, which is promising for Heusler alloys-based giant magneto resistance (GMR).

In this context, we present a theoretical study to invstigate the electronic and magnetic properties of $Fe_{3-x}Cr_xSi$ alloys for a wide range of Cr concentration ($0.25 \leq x \leq 2.75$). The rest of the paper is organized as follows: Sect. 2 includes the method of calculation, Sect. 3 is devoted to the results and discussions, and Sect. 4 contains the conclusions.

Method of calculation

The calculations are performed using density functional theory (DFT) [15] based on full-potential linearized-augmented plane-wave (FP-LAPW) [16] method (WIEN2K package). The electronic exchange-correlation potential is described within the generalized-gradient approximation (GGA) parameterized by Perdew et al. [17]. The calculations are performed using a supercell of 16 atoms for the $L2_1$ and A15 structures. In these calculations the core states are treated fully relativistically, while the semi-core and valence states are treated by the scalar relativistic approximation. The basis set parameters are: a 16 Ry cutoff energy for the plane waves in the interstitial region between the muffin tins and 169 Ry for the potential. The wavefunction expansion inside the muffin tins are taken up to $l_{max} = 10$ and the potential expansion up to $l_{max} = 4$. The core energy cutoff is taken as -6.0 Ry. The k-point sampling in the irreducible part of the Brillouin zone is performed using ($12 \times 12 \times 12$) Monkhorst Pack grid. The structures are fully relaxed until the forces on the atoms reach values less than 2 mRy/a.u. The convergence of the total energy in the self-consistent calculations is taken with respect to the total charge of the system with a tolerance 0.0001 electron charges. The electronic structure calculations to obtain the partial densities of states (DOS) for all structures are performed using the tetrahedron method with Blöchl corrections [18].

Results and discussion

The structural, electronic, and magnetic properties are investigated for $Fe_{3-x}Cr_xSi$ ternary alloys with Cr concentration x ranging from 0.25 to 2.75 in steps of 0.25. The Fe_3Si and Cr_3Si parent binary alloys with DO3 closed packed and A15 open structures, respectively, are presented in Fig. 1. Both alloys exhibit metallic behaviors, however, Fe_3Si is known to be ferromagnetic [7], whereas Cr_3Si is a typical Pauli paramagnet [4, 19]. This difference in their geometrical and magnetic structures suggest a diversity in the geometrical and magnetic structures of $Fe_{3-x}Cr_xSi$ ternary alloys.

Structural properties and energetics

Table 1 presents the structural parameters (lattice constant a; bulk modulus B), the formation energies, E_f, and the

Table 1 The lattice constants a, bulk modulus B and formation energies E_f of $Fe_{3-x}Cr_xSi$ alloys in their $L2_1$ and A15 structures and the energy difference $\Delta E = E_{L2_1} - E_{A15}$

x	a (Å)		B (GPa)		E_f (eV/f.u.)		ΔE (meV/f.u.)
	$L2_1$	A15	$L2_1$	A15	$L2_1$	A15	
0.25	5.60	4.50	193	185	−1.228	−0.944	−227
0.50	5.58	4.46	244	223	−1.215	−0.785	−428
0.75	5.58	4.50	243	196	−1.056	−0.958	−100
1.00	5.59	4.50	239	205	−1.010	−0.997	−12
1.25	5.60	4.50	237	212	−1.006	−0.955	−52
1.50	5.61	4.50	227	223	−0.978	−0.842	−136
1.75	5.61	4.50	256	224	−0.943	−0.952	+8
2.00	5.62	4.50	256	237	−0.848	−0.952	+752
2.25	5.65	4.50	219	231	−0.810	−1.070	+264
2.50	5.67	4.50	247	249	−0.912	−1.985	+572
2.75	5.68	4.50	248	249	−0.794	−1.24	+552

total energy difference between $L2_1$ and A15 structures for $Fe_{3-x}Cr_xSi$ alloys. From this table one can notice that the lattice constant is slightly increasing as a function of x in the case of $L2_1$ structure. This can be related to the larger atomic radius of Cr as compared to Fe, which causes an increase in the lattice constant by increasing Cr concentration due to the closed packed structure of $L2_1$ phase. However, the lattice constant is found to be independent of the Cr concentration in the case of A15 phase due to its open structure that permits Cr to substitute Fe without an expansion in the lattice constant. The bulk modulii of $Fe_{3-x}Cr_xSi$ alloys in their $L2_1$ phase are found to be larger than those with A15 phase for $x \leq 2$ and the opposite holds for larger concentrations.

By comparing the total energies of $L2_1$ and A15 structures, we found that the $L2_1$ structure is stable up to $x = 1.50$, beyond which A15 structure becomes more stable, see Table 1. In addition, we found that the formation energy decreases as a function of concentration for the alloys with the stable $L2_1$ phase . However, the alloys at higher concentrations ($x > 1.50$) with the A15 stable structure exhibit an increase in the formation energy. This indicates that the stability of $L2_1$ phase, in the range of $0.25 \leq x \leq 1.50$, increases for rich Fe alloys. However, in the range of $1.75 \leq x \leq 2.75$ (A15 phase), the stability increases for rich Cr alloys. It should be mentioned here that the total energy calculations gives an indication of a possible phase transformation between $L2_1$ and A15 geometrical structures upon alloying one parent binary alloy by the transition metal of the other. However, one should keep in mind that this result is inconclusive for the phase stability. To reach a closure, one has to test all possible geometrical structure and finalize by performing phonon calculations, which will be the subject of a future work.

Total and local magnetic moments

In this subsection we present the total and local magnetic moments of the two phases, $L2_1$ and A15, of $Fe_{3-x}Cr_xSi$ alloys, see Table 2. The total magnetic moment is found to decrease in the case of $L2_1$ phase until it reaches zero at $x = 2.00$, exhibiting a nonmagnetic state. Higher concentrations, however, exhibit negative total magnetic moments, see Fig. 2. To understand this behavior, one has to recall the Slater-Pauling rule for total magnetic moments that obeys the following equation [13, 20]:

$$M_{\text{tot}} = (N_v - 24n_{\text{Si}})\,\mu_{\text{B}} \quad (1)$$

where N_v is the number of valence electrons and n_{Si} is the number of Si atoms in each cell. We found that structures with Cr concentrations in the range $1.00 \leq x \leq 1.5$ exhibit

Table 2 The total magnetic moment M_{tot}, and local magnetic moments for $Fe_{3-x}Cr_xSi$ structures with $L2_1$ phase for $0.25 \leq x \leq 2.75$

x	M_{tot} (μ_B)	μ_{Fe} [A, C] (μ_B)	μ_{Fe} [B] (μ_B)	μ_{Cr} [A, C] (μ_B)	μ_{Cr} [B] (μ_B)	μ_{Si} [D] (μ_B)
0.25	14.6	0.85	2.57	–	0.44	−0.03
0.50	11.93	0.61	2.72	–	0.98	−0.03
0.75	9.98	0.44	2.74	–	1.23	−0.03
1.00	8.00	0.260	–	–	1.42	−0.03
1.25	6.00	0.23	–	−0.64	1.34	−0.01
1.50	4.00	0.15	–	−0.94	1.23	−0.01
1.75	1.41	0.07	–	−0.25	0.50	−0.01
2.00	0.00	0.00	–	0.00	0.00	0.00
2.25	−1.99	0.01	–	−0.95	0.73	0.00
2.50	−3.74	0.06	–	−1.02	0.78	0.00
2.75	−5.14	0.34	–	−1.20	0.78	0.00

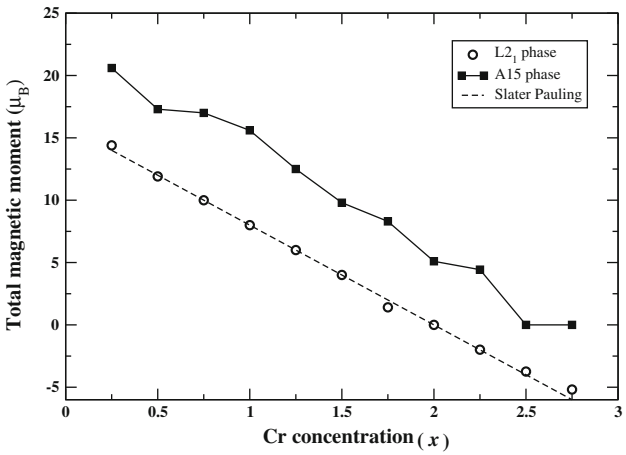

Fig. 2 The total magnetic moment as a function of Cr concentration for the $L2_1$ and A15 phases in comparison with Slater-Pauling curve

integer total magnetic moments obeying the Slater-Pauling rule. At $x = 2.00$ we obtained a nonmagnetic state, which lies on the border of Slater-Pauling rule. The number of valence electrons in the cell of this alloy is 24/f.u., which leads to a zero total magnetic moment according to Eq. 1. In contrast, the remaining Cr concentrations exhibit non-integer total magnetic moments that are found to be slightly off the Slater-Pauling curve, Fig. 2. For the A15 phase, however, one can see a monotonic decrease of the total magnetic moment until it reaches zero at $x = 2.50$. In this phase all structures exhibit non-integer total magnetic moments, with values higher than the case of the $L2_1$ phase, see Fig. 2. The ferromagnetic to nonmagnetic transition in our calculations occurs at $x = 2.50$, whereas, it takes place experimentally at $x = 2.70$ [9].

In Tables 2 and 3, we present the total as well as the local magnetic moments of the alloys in their $L2_1$ and A15 phases, respectively. These tables show complex magnetic structures of the alloys in both phases. In Table 2 one can see that Fe atoms at [A, C] sites are lower than the corresponding values obtained in a previous study for Fe_3Si binary alloy ($1.29\mu_B$) [7]. This can be related to the substitution of some Fe atoms by Cr at [B] sites. However, the magnetic moments of the rest of Fe atoms at [B] sites remain almost the same as those in Fe_3Si parent alloy. The local magnetic moments of Fe atoms at [A, C] sites continue to decrease as Cr concentration increases, whereas those of Cr at [B] sites increase. The larger magnetic moments of Fe atoms at [B] sites is related to the proximity of Fe nearest neighboring atoms at [A, C] sites. In contrast the first neighbors of Fe atoms at [A, C] sites are Cr and Si atoms, which causes a reduction in their moments due to the hybridization with Si p and Cr d bands. Beyond $x = 1$, Cr atoms start to occupy [A, C] sites with local magnetic moments coupled antiferromagnetically with those of Cr atoms at [B] sites. The overall effect of these changes causes a decrease in the total magnetic moment until it reaches zero at $x = 2$, then continues to increase with negative total magnetic moment as Fe atoms at [A, C] sites starts to couple antiferromagnetically with those of Cr at [B] sites. In Table 3 we find that the local magnetic moments of Fe atoms close to Cr atoms have smaller values than those on their original sites. This reduction is related to the hybridization between Cr and Fe d bands. For Cr atoms, the local magnetic moment is found to decrease as a function of Cr concentration. The Si atoms, however, exhibit negligibly small induced magnetic moments.

Table 3 The total magnetic moment M_{tot}, and local magnetic moments for $Fe_{3-x}Cr_xSi$ structures with A15 phase for $0.25 \leq x \leq 2.75$

x	M_{tot} (μ_B)	μ_{Fe} (μ_B)	μ_{Cr} (μ_B)	μ_{Si} (μ_B)
0.25	20.57	1.64, 2.14, 2.57	−0.74	−0.07
0.50	17.26	1.09, 1.99	−0.19	−0.06
0.75	17.00	1.56, 2.02	−0.03, 0.09	−0.05
1.00	15.64	1.96	0.08	−0.046
1.25	12.48	1.23, 1.83, 1.96	0.0, 0.05	−0.04
1.50	9.83	1.05, 1.81	0.11, 0.16	−0.03
1.75	8.25	1.13, 1.57, 1.85	−0.02, 0.05, 0.30	−0.02
2.00	5.10	1.14	0.06, 0.08	−0.01
2.25	4.43	1.24, 1.86	0.09, −0.48	−0.01
2.50	0.00	0.00	0.00	0.00
2.75	0.00	0.00	0.00	0.00

Density of states

It has been found earlier that there is an intimate relation between the integer total magnetic moments and the half metallicity behavior, which is also the case of this study. To reveal this fact we present the DOS for six systems of Cr concentration $x = 0.25$ up to $x = 1.50$ in their $L2_1$ phase, see Fig. 3. In this figure one can notice the metallic behavior of the structures with Cr concentrations of $x = 0.25$, 0.50, and 0.75, with spin polarisations P of 42, 96, and 98%, respectively, calculated at the Fermi level using the following equation:

$$P = (N_\uparrow - N_\downarrow)/(N_\uparrow + N_\downarrow) \quad (2)$$

where $N_\uparrow$ and $N_\downarrow$ represent the density of states at the Fermi level for the majority and minority spin channels, respectively. One can also see that the $Fe_{3-x}Cr_xSi$ structure with $x = 1.00$, 1.25 and 1.50 exhibit spin polarizations of 100% due to the absence of the electronic states in their minority spin channels. The Fe_2CrSi Heusler alloy, which has a perfect stoichiometric composition exhibits an indirect band gap of 0.60 eV along the Γ–X symmetry line. This value is higher than that obtained by Hongzhi et al. (0.42 eV) [11], which may be related to using the local spin density approximation rather than the GGA used in the present study to describe the exchange-correlation potential. Our calculated total magnetic moment of 8.00 μ_B/cell (2.00 μ_B/f.u.) agrees with the theoretical and experimental values obtained by Hongzhi et al. [11] of 2.00 and 2.05 μ_B/f.u., respectively, whereas it is slightly higher than the value obtained by Yoshimura et al. [12] of 1.98 μ_B/f.u. This full Heusler alloy is believed to be promising for potential applications in spintronics due to several reasons. Firstly, it has a high Curie temperature of 520 K [11]. Second, it is robust against defects [21]. Third, it exhibits a van-Hove singularity of the density of states at the Fermi level in the majority spin channel and an appreciable band gap in the minority spin channel with the Fermi level in the middle of the energy gap. These properties suggest this

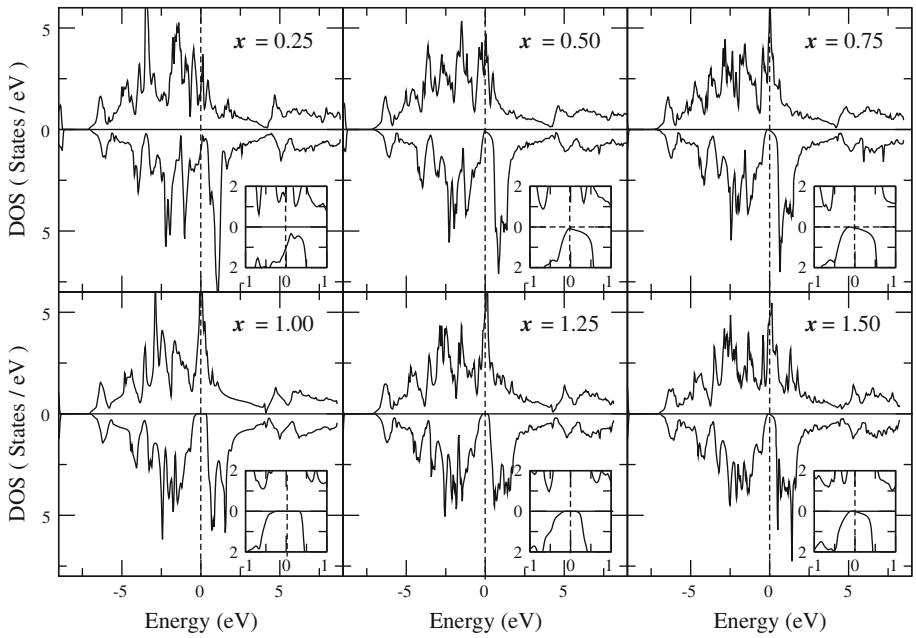

Fig. 3 The total density of states (DOS) for the $Fe_{3-x}Cr_xSi$ with Cr concentrations $0.25 \leq x \leq 1.50$ in the stable $L2_1$ phase

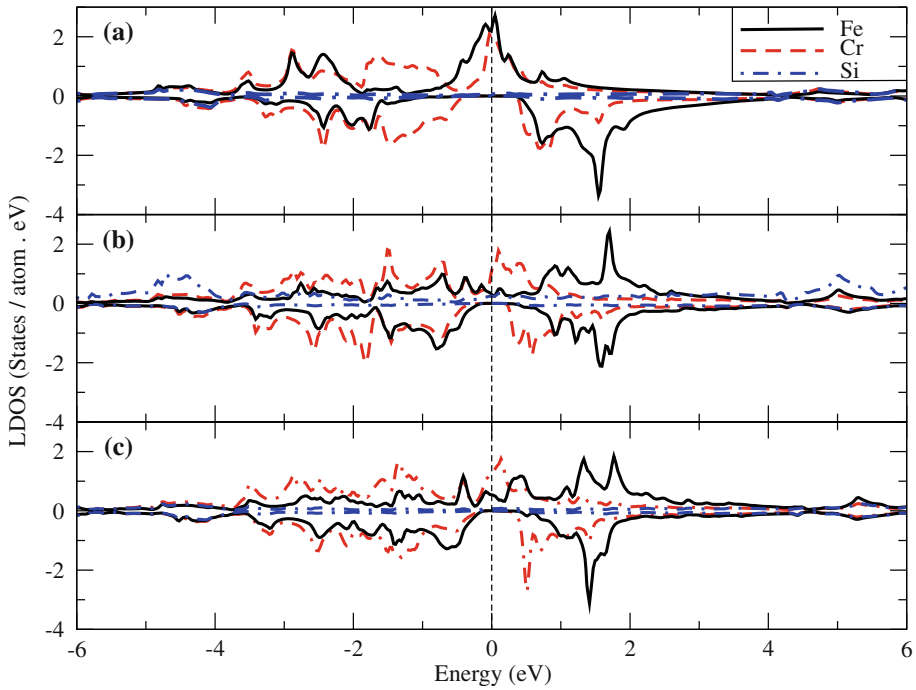

Fig. 4 (Color online) The local density of states for the $Fe_{3-x}Cr_xSi$ half-metallic structures with their stable $L2_1$ phase at: **a** $x = 1.00$. **b** $x = 1.25$. **c** $x = 1.50$

alloy as a very good candidate for tunneling magnetoresistance (TMR) devices [22].

For the higher concentrations at $x = 1.25$ and 1.50, the band gaps are found to be lower than the ideal Fe_2CrSi Heusler alloy, namely 0.24 and 0.21 eV, respectively. This reduction in the values of the band gaps can be interpreted using Fig. 4, which presents the local density of states (LDOS) for $x = 1.00$, 1.25, and 1.50 concentrations. From this figure one can notice the energy shift of the Fe bonding and Cr antibonding states toward higher and lower energies, respectively, which causes a decrease in the band gaps of the alloys with $x = 1.25$ and 1.50.

For a better understanding of the covalent bonding in $L2_1$ and A15 phases, we plot the LDOS of two selected systems at $x = 1.00$, and 2.00 for both phases. In Fig. 5, we present the LDOS for the doped alloy in its $L2_1$ phase with Cr concentration $x = 1.00$ from which one can see a wide band gap in the minority channel of the LDOS, indicating a strong covalent bond between Fe and Cr *d* states. However, for the A15 phase, the wide band gap is absent, which

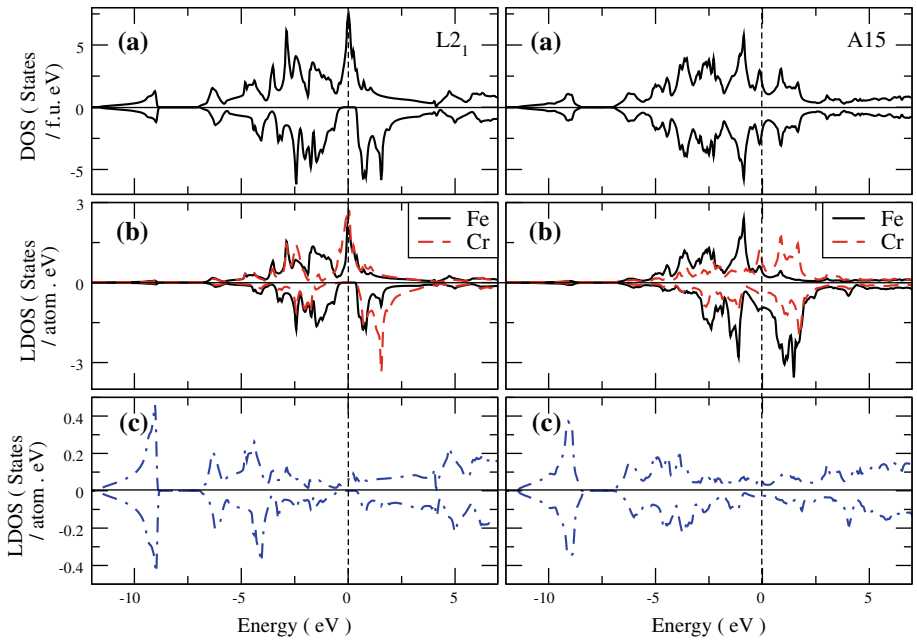

Fig. 5 (Color online) The total and local density of states for Fe_2CrSi alloy in the $L2_1$ phase (*left*) and A15 phase (*right*). **a** total DOS. **b** Fe and Cr LDOS. **c** Si LDOS

means that the covalent bond becomes weaker. For $FeCr_2Si$ alloy, however, there are no band gaps in the DOS neither for $L2_1$ nor for A15 phases, which means weak covalent bonds in both phases (see Fig. 6). The minority and majority DOSs of the $L2_1$ phase are found to be equal in Fig. 6, which leads to the nonmagnetic state. The A15 phase, however, is found to be magnetic as can be seen from its DOS. The magnetic interaction in the case of A15 phase may be the reason for the stabilization of this phase as compared to $L2_1$ phase.

Conclusions

We performed DFT calculations using FP-LAPW method and GGA to investigate the structural, electronic and magnetic properties of $Fe_{3-x}Cr_xSi$ alloys with $0.25 \leq x \leq 2.75$ and steps of 0.25. We found that the $L2_1$ phase is more stable than A15 phase for Cr concentration $x \leq 1.50$, whereas, the opposite holds for higher concentrations. The structures with the stable $L2_1$ phase are found to exhibit a metallic behavior for $x = 0.25$, 0.50, and 0.75 with spin

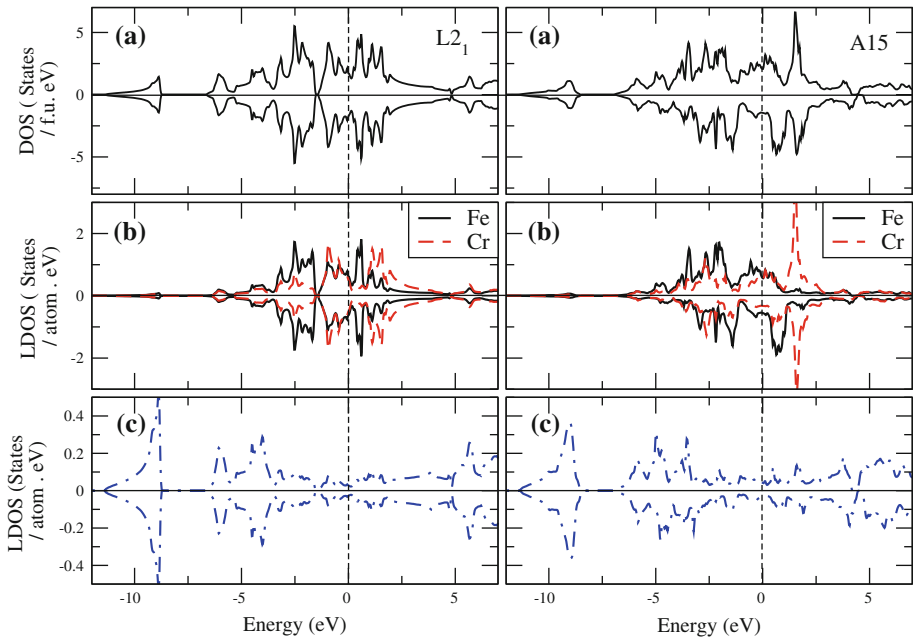

Fig. 6 (Color online) The total and local density of states for $FeCr_2Si$ alloy in the $L2_1$ phase (*left*) and A15 phase (*right*). **a** total DOS. **b** Fe and Cr LDOS. **c** Si LDOS

polarizations of 42, 96, and 98%, respectively. However, they exhibit a half metallic behavior at $x = 1.00$, 1.25, and 1.50 with band gaps of 0.60, 0.24, and 0.21 eV, respectively. In contrast, all A15 structures are found to exhibit metallic behaviors. The total magnetic moments are found to decrease in the case of $L2_1$ phase from 14.4 μ_B/cell at $x = 0.25$ to zero at $x = 2.00$, beyond which they become negative with non-integer values for the metallic structures and integer values for the half-metallic. However, a monotonic decrease is found for the case of A15 phase with values larger than those of $L2_1$ phase until they reach zero at $x = 2.50$.

Acknowledgements Bothina Hamad and Jamil Khalifeh thank the University of Jordan for the financial support during their sabbatical leaves. Qing-Miao Hu acknowledges the financial support from the NSFC under Grant No. 50871114.

References

1. Jorgensen J-E, Rasmussen SE (1982) Acta Cryst B 38:346
2. Wijn HPJ (1991) Magnetic properties of metal, d-elements, Alloys and compdounds, Springer-Verlag, Berlin, p 146
3. Jorgensen J-E, Axe JD, Corliss LM, Hastings JM (1982) Phys Rev B 25:5856
4. Mihailov IG, Pan WM, Shevtshenko AD, Ber G (1979) Solid State Phys 21:2797
5. Villars P, Calvert LD (1985) In: Pearsons handbook of crystallographic data for intermetallic phases. American Society for Metals, Materials Park
6. Zukowski E, Andrejczuk A, Dobrzynski L, Kaprzyk S, Cooper MJ, Duffy JA, Timms DN (2000) J PhysCondens Matter 12:7229
7. Hamad B, Khalifeh J, Abu Aljarayesh I, Demangeat C, Luo H, Hu O-M (2010) J Appl Phys 107:093911
8. Nakamura Y (1988) Landolt-Börnstein New Series III/19c, chap. 1. Springer, Berlin, p 26
9. Zaleski P, Biernacka M, Dobrzyński L, Perzyńska K, Rećko K (2003) Phys Stat Sol (a) 196:260
10. Goripati HS, Furubayashi T, Karthik SV, Nakatani TM, Takahashi YK, Hono K (2011) J Appl Phys 109:043901
11. Hongzhi L, Zhiyong Z, Li M, Shifeng X, Heyan L, Jingping Q, Yangxian L, Guangheng W (2007) J Phys D Appl Phys 40:7121
12. Yoshimura S, Asano H, Nakamura Y, Yamaji K, Takeda Y, Matsui M, Ishida S, Nozaki Y, Matsuyama K (2008) J Appl Phys 103:07D716
13. Galanakis I, Dederichs PH, Papanikolaou N (2002) Phys Rev B 66:174429
14. Ko V, Qiu J, Luo P, Han GC, Feng YP (2011) J Appl Phys 109:07B103
15. Kohn W, Sham LJ (1965) Phys Rev 140:A1133
16. Blaha P, Schwarz K, Madsen G, Kvasnika D, Luitz K (2001) WIEN2k, Technical Universität Wien, ISBN 3-9501031-1-2
17. Perdew JP, Wang Y (1992) Phys Rev B 45:13244
18. Blöchl PE, Jepsen O, Andersen OK (1994) Phys Rev B 49:16223
19. Jorgensen JE, Rasmussen SE (1979) J Cryst Growth 47:124
20. Hülsen B, Scheffler M, Kratzer P (2009) Phys Rev B 79:094407
21. Hamad BA (2011) Eur Phys J B 80:11
22. Sakuraba Y, Hattori M, Oogane M, Ando Y, Kato H, Sakuma A, Miyazaki T, Kubota H (2006) Appl Phys Lett 88:192508